IEEE Access
Multidisciplinary | Rapid Review | Open Access Journal

Received January 9, 2022, accepted February 8, 2022, date of publication February 16, 2022, date of current version February 28, 2022.

Digital Object Identifier 10.1109/ACCESS.2022.3152155

Position Control Considering Slip Motion of Tracked Vehicle Using Driving Force Distribution and Lateral Disturbance Suppression

HIROAKI KUWAHARA[1,2], (Member, IEEE), AND TOSHIYUKI MURAKAMI[3], (Senior Member, IEEE)

[1]Graduate School of Science and Technology, Keio University, Yokohama 223-8522, Japan
[2]Toshiba Corporation, Yokohama 235-0017, Japan
[3]Department of System Design Engineering, Keio University, Yokohama 223-8522, Japan

Corresponding author: Hiroaki Kuwahara (kuwahara@sum.sd.keio.ac.jp)

This work was supported in part by the KEIRIN JKA under Grant 2021-M128.

ABSTRACT Complex slippage and nonholonomic constraints can disturb the precise movement of tracked vehicles. In this study, a position control system using driving force control and virtual-turning velocity control (VTVC) was established for a tracked vehicle. Slippage in the translational direction can be suppressed by controlling the driving force of the crawlers, estimated using the vehicle velocity. However, the driving forces interfere with each other in a turning motion. Therefore, a driving force distribution method was developed using the instantaneous turning center of a vehicle to decouple the forces. This distribution induced slippage in the direction of turning. In addition, a virtual reference was derived from the vehicle velocity and lateral disturbance, which described the effects of the nonholonomic constraints and skidding of the tracked vehicle. Next, a VTVC method was developed to suppress the lateral disturbance by controlling the turning velocity to follow the virtual reference. The experimental results confirm that the proposed approach ensures high-performance position tracking and adequate slippage of the tracked vehicle.

INDEX TERMS Autonomous vehicles, driving force control, machine learning, observers, position control.

I. INTRODUCTION

A tracked vehicle can traverse diverse terrains because its crawlers ensure ground contact while traveling [1]–[5]. However, two significant disturbances to tracked vehicles hinder precise movement: 1) complex slippage of the crawler on the ground and 2) nonholonomic constraints of vehicle motion. Therefore, motion control for tracked vehicles must reflect slippage and nonholonomic constraints to ensure precise position control.

Compared to wheeled automobiles, tracked vehicles slip more frequently and are difficult to model. Various simulators describe the motion mechanisms of tracked vehicles, including slippage [6], [7]. A model and Kalman filter [8] can be employed to estimate the slippage of tracked vehicles and automobiles in real time. A multisensor fusion of location data and inertial measurements [9] and image processing [10] can also be applied. Several methods, such as backstepping [11], sliding mode control [12], model predictive control [13], observer-based robust control [14], and trajectory planning [15], have been proposed to handle slippage. These methods ensure system robustness against slippage but do not suppress slippage. Slippage is related to the frictional force acting between the crawler and the ground surface [16], [17], and it corresponds to the crawler driving force. Hence, slippage can be suppressed by controlling the driving force. Although the driving force control of automobiles has been investigated [18]–[21], few studies have considered tracked vehicles. The driving force has been estimated using observers based on the axle velocity [21], neglecting the slippage effect. In addition, the driving forces of the crawlers interfere with each other while controlling tracked vehicles using driving force feedback. Therefore, the driving force distribution that decouples the driving forces must be considered. The decoupled driving forces provide the necessary moment for turning. However, slippage can be induced in the direction of turning. Although this slippage facilitates the lateral movement of the tracked vehicle, it interferes

The associate editor coordinating the review of this manuscript and approving it for publication was Pasquale De Meo.

with motion control, such as positioning. In addition, nonholonomic constraints are established in conventional mobile robots to nullify commands in the lateral direction. Recently, the effectiveness of position control, including a compensator for the effects of nonholonomic constraints, has been demonstrated for a wheeled mobile robot [22]. For tracked vehicles, an improvement in position control can be expected by suppressing the disturbance caused by the nonholonomic constraints while allowing adequate slippage.

We have previously developed a method for estimating vehicle velocity, including slippage, using a disturbance observer (DOB) and machine learning [23]. Moreover, we have established a driving control system based on the estimated driving force [24]. When turning is performed while controlling the driving force, the interference between the driving forces of the crawlers prevents motion. Therefore, a driving force distribution that induces slippage in the turning direction by decoupling the driving forces is developed in this study. We designed the distribution based on the instantaneous center of the vehicle. In addition, we analyzed the lateral disturbance of the tracked vehicle, adopting the skidding and nonholonomic constraints as the equivalent lateral disturbance. The equivalent lateral disturbance is estimated using a workspace observer (WOB) [25], [26], coordinate transformation, and selection matrix. Moreover, a virtual-turning velocity reference was derived from the equivalent lateral disturbance and vehicle velocity. Hence, a virtual-turning velocity control (VTVC) method was established to suppress the equivalent lateral disturbance by ensuring that the actual turning velocity followed the virtual-turning velocity reference. A position control system was constructed by integrating the position control, driving force distribution, and VTVC. The resulting control system ensures high-performance position tracking by suppressing the lateral disturbance while allowing the tracked vehicle to slip appropriately. The proposed control method was validated experimentally.

The contributions of this study are as follows. 1) The proposed method controls the driving force estimated from the vehicle velocity, including slippage, to suppress slippage in the translational direction. 2) The proposed driving force distribution method decouples the interference of the crawler driving forces, induces adequate slippage in the turning direction, and improves the turning performance. 3) The proposed position control improves the lateral positioning performance while allowing for slippage in the turning direction induced by the distribution.

The remainder of this paper is organized as follows. Section II presents details of the tracked vehicle model. Section III describes the estimation and distribution of the driving forces. In Section IV, the position control with driving force distribution and VTVC is introduced. Section V presents the experimental results for the turning performance based on the proposed driving force distribution and the effects of the VTVC. Finally, we present the conclusions in Section VI.

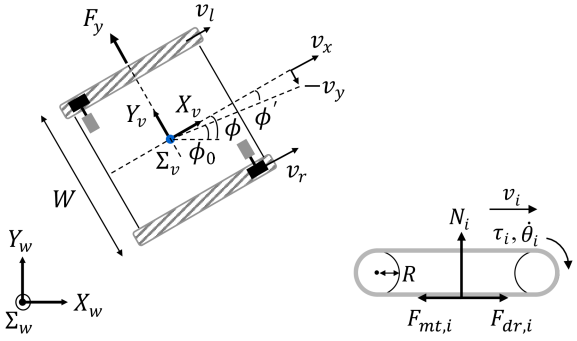

(a) Top view (b) Side view

FIGURE 1. Tracked vehicle model.

TABLE 1. Parameters of the tracked vehicle model.

Parameters	Descriptions
Σ_w (X_w, Y_w)	World coordinates
Σ_v (X_v, Y_v)	Vehicle coordinates
i	Motor ID (r: right, l: left)
W	Thread
R	Sprocket radius
ϕ	Turning angle with slip angle
ϕ_0	Turning angle without slip angle
ϕ'	Slip angle
v_x	Vehicle translational velocity
v_y	Lateral slip velocity
F_y	Lateral force
v_i	Crawler velocity
τ_i	Motor torque
$\dot{\theta}_i$	Motor velocity
N_i	Normal force on crawler
$F_{mt,i}$	Force on road surface due to motor torque
$F_{dr,i}$	Driving force

II. TRACKED VEHICLE MODEL

Fig. 1 shows the tracked vehicle model, and Table 1 lists the model parameters. In Fig. 1 (a), the origin of the vehicle coordinates is the center of the vehicle. The axes are aligned in the translational and lateral directions of the vehicle. Position vector $\boldsymbol{x}$ representing the position (x, y) and turning angle (ϕ) of the vehicle in the world coordinates is defined by $\boldsymbol{x} = \begin{bmatrix} x & y & \phi \end{bmatrix}^T$. The turning angle is defined by $\phi = \phi_0 + \phi'$.

The kinematics of the tracked vehicle is expressed as

$$\dot{x}\cos\phi + \dot{y}\sin\phi = v_x, \tag{1}$$

$$\dot{x}\sin\phi - \dot{y}\cos\phi = v_y. \tag{2}$$

The kinematic relationship between the vehicle velocity and crawler velocity is

$$v_x + \frac{W}{2}\dot{\phi} = v_r = (1-\lambda_r)R\dot{\theta}_r, \tag{3}$$

$$v_x - \frac{W}{2}\dot{\phi} = v_l = (1-\lambda_l)R\dot{\theta}_l, \tag{4}$$

where λ_i is the slip ratio, which represents the slip between the crawler and the road surface or between the sprocket and the crawler.

The equations of motion of the vehicle are given by

$$m\dot{v}_x = F_{dr,r} + F_{dr,l}, \tag{5}$$

$$m\dot{v}_y = F_y, \tag{6}$$

$$J_v\ddot{\phi} = \frac{W}{2}(F_{dr,r} - F_{dr,l}), \tag{7}$$

where m and J_v are the mass and moment of inertia of the vehicle, respectively. When the vertical pressure at the crawler contact surface is constant, the driving force can be quasi-experimentally expressed as follows [16], [17]:

$$F_{dr,i} = N_i\mu f(\lambda_i, k, L), \tag{8}$$

where μ and $f(\lambda_i, k, L)$ are the dynamic friction coefficient and a function with the slip ratio λ_i, shear displacement coefficient k, and crawler length L as arguments, respectively.

From Fig. 1 (b), the equation of motion of the crawler is

$$J_m\frac{\dot{v}_i}{R^2} = F_{mt,i} - F_{dr,i}, \tag{9}$$

where J_m is the motor-shaft conversion moment of inertia. Thus, the tracked vehicle is moved by the driving force that simultaneously behaves as a disturbance and acts on the motor.

III. ESTIMATION AND DISTRIBUTION OF DRIVING FORCE

A. TRANSLATIONAL VELOCITY ESTIMATION NEURAL NETWORK

The crawler velocity, including slippage, was considered to estimate the driving force. We used a translational velocity estimation neural network (TVNN) to estimate the vehicle translational velocity [24]. The TVNN architecture is shown in Fig. 2. In Fig. 2, the hat symbol above a variable denotes the estimated value, and $\hat{\tau}_r^{dis}$ and $\hat{\tau}_l^{dis}$ are the disturbances to the right and left crawler motors, respectively, as estimated by a DOB [27], [28]. The inputs of the TVNN, except the estimated disturbance, namely, the motor velocities and translational acceleration, can be measured using the motor encoders and an accelerometer, respectively. Generally, motor disturbances include the reaction force applied to the motor by the ground surface when a driving force is generated. The reaction force includes the driving force related to the slip ratio, as expressed by (8). Therefore, the estimated disturbance reflects the nonlinear and complex slip information and is used as an input for the TVNN. The TVNN is a two-layer feedforward neural network. The hyperbolic tangent sigmoid and linearized transfer functions were used as the activation functions of the hidden and output layers, respectively. The TVNN can be trained using supervised machine learning or other methods. The trained TVNN estimates the translational velocity $\hat{v}_x$. By substituting the translational velocity $\hat{v}_x$ and turning velocity $\dot{\phi}$ (measured using a gyroscope) into the inverse kinematics, the estimated crawler velocity $\hat{v}_i$ is obtained as

$$\hat{v}_i = \begin{cases} \hat{v}_x + \dfrac{W}{2}\dot{\phi}, & (i = r) \\ \hat{v}_x - \dfrac{W}{2}\dot{\phi}, & (i = l). \end{cases} \tag{10}$$

Here, the crawler velocity in the translational direction was estimated, considering the slippage in the direction of turning.

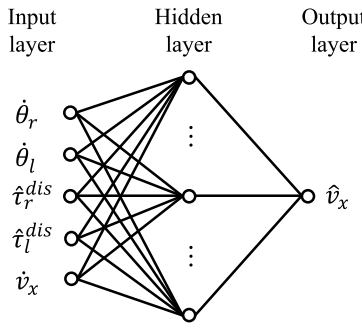

FIGURE 2. Architecture of the TVNN.

B. DRIVING FORCE OBSERVER

A driving force observer (DFOB) [23] was designed to estimate the driving force based on the estimated crawler velocity. A block diagram of the DFOB is presented in Fig. 3. The driving force estimated by the DFOB is expressed as

$$\hat{F}_{dr,i} = \frac{g_{DF}}{s + g_{DF}}(F_{mt,i} - sJ_{mn}\frac{\hat{v}_i}{R^2}), \tag{11}$$

where J_{mn} and g_{DF} are the nominal motor-shaft conversion moment of inertia J_m and DFOB cutoff frequency, respectively. The DFOB provides the driving force as a low-pass filtered value of the driving force calculated using (11). The driving force required for motion can be generated via feedback control of the estimated driving force, and slippage in the translational direction of the crawler can be suppressed.

C. DRIVING FORCE DISTRIBUTION

When controlling the vehicle turning and driving force simultaneously, generating the moment necessary for turning is difficult because the right and left driving forces interfere with each other. Thus, we distribute the driving force based on the inverse kinematics solution using a weight matrix. For a typical two-wheeled mobile robot, Jacobian matrix $\boldsymbol{J}$, which establishes the relationship between the motor velocities ($\dot{\theta}_r$, $\dot{\theta}_l$) and vehicle velocities (v_x, $\dot{\phi}$), transforms into the following square matrix:

$$\begin{bmatrix} v_x \\ \dot{\phi} \end{bmatrix} = \boldsymbol{J}\begin{bmatrix} \dot{\theta}_r \\ \dot{\theta}_l \end{bmatrix}, \tag{12}$$

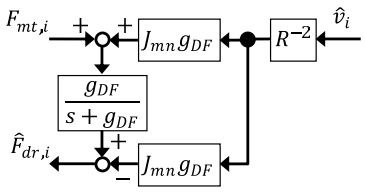

FIGURE 3. Block diagram of the DFOB.

$$\boldsymbol{J} = \begin{bmatrix} \frac{R}{2} & \frac{R}{2} \\ \frac{R}{W} & -\frac{R}{W} \end{bmatrix}. \tag{13}$$

By time-differentiating both sides of (13), the relationship between the motor accelerations ($\ddot{\theta}_r$, $\ddot{\theta}_l$) and vehicle accelerations ($\dot{v}_x$, $\ddot{\phi}$) can be derived. When the total driving force is calculated using the vehicle accelerations, the inverse Jacobian matrix $\boldsymbol{J}^{-1}$ can be used to evenly distribute the driving forces between the crawlers. However, the distribution causes interference from crawler driving forces. A weight matrix was introduced to design the distribution, as follows:

$$\boldsymbol{w} = diag\begin{bmatrix} w_r & w_l \end{bmatrix}. \tag{14}$$

Next, the driving force can be represented by the weight matrix and inverse Jacobian matrix, as follows:

$$\begin{bmatrix} F_{dr,r} \\ F_{dr,l} \end{bmatrix} = \frac{1}{R}\boldsymbol{w}\boldsymbol{J}^{-1}\begin{bmatrix} \dot{v}_x \\ \ddot{\phi} \end{bmatrix}. \tag{15}$$

From (15), the weight matrix elements, w_r and w_l, are equivalent to the virtual inertias of the right and left crawlers, respectively. Therefore, by designing the weight matrix, the driving force reference of the crawler can be determined, and the force is distributed from the acceleration reference generated by the position controller.

The weight matrix design involves the instantaneous turning center of the vehicle, as shown in Fig. 4. A line parallel to the Y_v-axis, drawn on the tracked vehicle from the center of rotation, is defined as a nonslip line [29]. The instantaneous turning center is defined as a point on the nonslip line, and the velocity along the X_v-axis at this point is the average of the crawler velocities. The position of the instantaneous turning center of the vehicle coordinates (${}^v x_{ic}$, ${}^v y_{ic}$) is obtained using

$${}^v x_{ic} = -\frac{v_y}{\dot{\phi}}, \tag{16}$$

$${}^v y_{ic} = \frac{v_x}{\dot{\phi}} - \frac{v_r + v_l}{2\dot{\phi}}. \tag{17}$$

The instantaneous turning center is handled as a virtual control point without slippage in the turning direction. In other words, in an actual situation, slippage in the turning direction

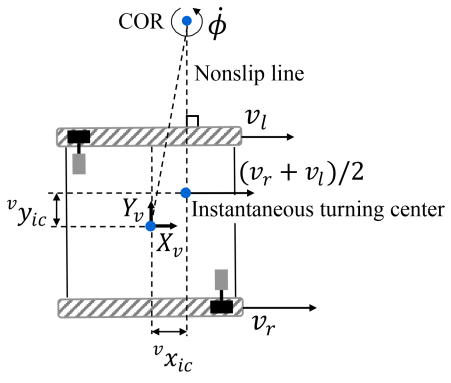

FIGURE 4. Instantaneous turning center (COR, center of rotation).

is induced by controlling at this point. The equation of motion for the rotational direction at the instantaneous turning center can be expressed as

$$J'_v\ddot{\phi} = \left(\frac{W}{2} + {}^v y_{ic}\right)F_{dr,r} - \left(\frac{W}{2} - {}^v y_{ic}\right)F_{dr,l} - F_y^v x_{ic}, \tag{18}$$

$$J'_v = J_v + \delta J_v,\ \delta J_v = m({}^v x_{ic}^2 + {}^v y_{ic}^2). \tag{19}$$

From (5), (18), and (19), the distributed driving force necessary for motion is expressed as

$$\begin{bmatrix} F_{dr,r} \\ F_{dr,l} \end{bmatrix} = \begin{bmatrix} m(\frac{1}{2} - \frac{{}^v y_{ic}}{W}) & \frac{J_v}{W} \\ m(\frac{1}{2} + \frac{{}^v y_{ic}}{W}) & -\frac{J_v}{W} \end{bmatrix}\begin{bmatrix} \dot{v} \\ \ddot{\phi} \end{bmatrix} + \begin{bmatrix} \frac{\delta J_v\ddot{\phi} + {}^v x_{ic}F_y}{W} \\ -\frac{\delta J_v\ddot{\phi} + {}^v x_{ic}F_y}{W} \end{bmatrix}. \tag{20}$$

From (20), if the instantaneous turning center does not deviate from the vehicle center along the lateral direction (${}^v y_{ic} = 0$), the driving force should be equally distributed among the crawlers. Otherwise (${}^v y_{ic} \neq 0$), the deviation should be represented by the weight of the crawler driving forces. Thus, we designed the elements of the weight matrix as follows:

$$w_r = m\left(\frac{1}{2} - \frac{{}^v y_{ic}}{W}\right), \quad (0 \leq w_r \leq 1), \tag{21}$$

$$w_l = m\left(\frac{1}{2} + \frac{{}^v y_{ic}}{W}\right), \quad (0 \leq w_l \leq 1). \tag{22}$$

The second term on the right-hand side of (20) indicates the disturbance in the world coordinates, compensated by the WOB, as described in Section IV.

IV. POSITION CONTROL

A. CONTROL SCHEME

In this study, the position control system of a tracked vehicle was designed to achieve the intended motion and ensure robustness against disturbances. The proposed position control system is shown in Fig. 5. The acceleration reference vector for the vehicle coordinates ($\dot{\boldsymbol{v}}$), crawler driving force vector ($\boldsymbol{F_{dr}}$), estimated crawler velocity vector ($\hat{\boldsymbol{v}}_i$), and crawler motor force vector ($\boldsymbol{F_{mt}}$) are defined as $\dot{\boldsymbol{v}} = \begin{bmatrix} \dot{v}_x & \ddot{\phi} \end{bmatrix}^T$, $\boldsymbol{F_{dr}} = \begin{bmatrix} F_{dr,r} & F_{dr,l} \end{bmatrix}^T$, $\boldsymbol{v}_i = \begin{bmatrix} \hat{v}_r & \hat{v}_l \end{bmatrix}^T$, and $\boldsymbol{F_{mt}} = \begin{bmatrix} F_{mt,r} & F_{mt,l} \end{bmatrix}^T$, respectively. The superscripts *cmd*, *res*, *ref*, and *dis* represent a command, response, reference, and disturbance, respectively. Matrices ${}^w\boldsymbol{R_v}$, ${}^v\boldsymbol{R_w}$, $\boldsymbol{S}$, and $\boldsymbol{T}$ are the transformation matrices from Σ_w to Σ_v and from Σ_v to Σ_w, the selection matrix, and the command conversion matrix, respectively. The control system comprises a position controller $\boldsymbol{C_p}(\boldsymbol{s})$, driving force controller $\boldsymbol{C_f}(\boldsymbol{s})$, and virtual-turning velocity controller $\boldsymbol{C_v}(\boldsymbol{s})$. The control system controls the position response ($\boldsymbol{x^{res}}$) in tracking the command ($\boldsymbol{x^{cmd}}$). A DOB and WOB were adopted to construct the position control system with robustness against disturbances to the tracked vehicle. The WOB was also used to estimate

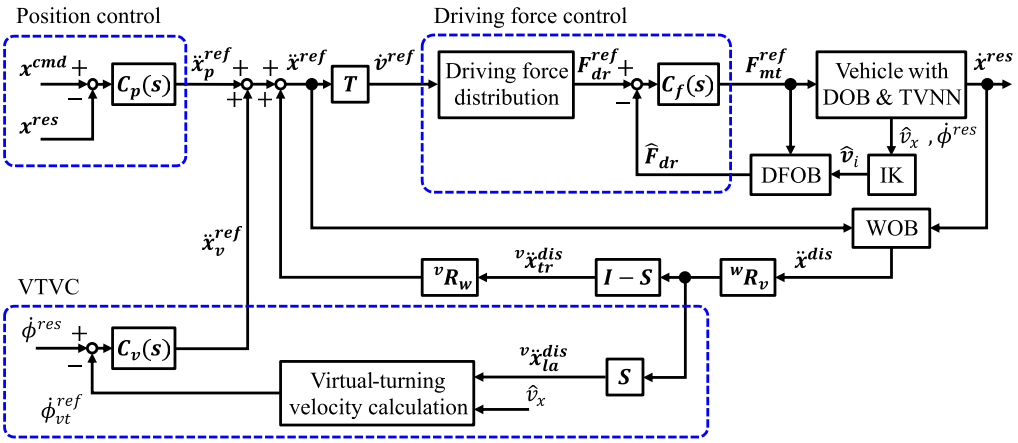

FIGURE 5. Structure of the proposed position control system (IK, Inverse Kinematics).

the lateral disturbance, equivalent to the effects of skidding and nonholonomic constraints. We define this disturbance as the equivalent lateral disturbance. Based on the relationship between the equivalent lateral disturbance and the translational velocity, a virtual-turning velocity reference was determined to suppress the disturbance.

B. POSITION CONTROL

The position controller in the world coordinates was designed as follows:

$$\ddot{\boldsymbol{x}}^{\boldsymbol{ref_p}} = [\ddot{x}^{ref}\ \ddot{y}^{ref}\ *]^T = \boldsymbol{C_p}(\boldsymbol{s})(\boldsymbol{x}^{\boldsymbol{cmd}} - \boldsymbol{x}^{\boldsymbol{res}}), \tag{23}$$

where $\ddot{\boldsymbol{x}}^{\boldsymbol{ref_p}}$, $\ddot{x}^{ref}$, and $\ddot{y}^{ref}$ represent the acceleration reference vector provided by the position controller and its X_w and Y_w direction components, respectively. The asterisk symbol is an unused variable. The X_w- and Y_w-direction components are controlled by the position controller. The turning angle in the acceleration reference vector is controlled by the VTVC described in Section IV-C. The position controller $\boldsymbol{C_p}(\boldsymbol{s})$ was designed using proportional-derivative control, as follows:

$$\boldsymbol{C_p}(\boldsymbol{s}) = \boldsymbol{K_{pp}} + s\boldsymbol{K_{pd}}, \tag{24}$$

where $\boldsymbol{K_{pp}}$ and $\boldsymbol{K_{pd}}$ are the proportional and derivative gains for the position, respectively.

C. VTVC BASED ON EQUIVALENT LATERAL DISTURBANCE

We compensated for the disturbances to the crawler motor, owing to the driving force and modeling errors using the DOB. Furthermore, we used the WOB to estimate disturbances to the vehicle in world coordinates (workspace). Fig. 6 shows a block diagram of the WOB. In Fig. 6, g_W indicates the WOB cutoff frequency. The WOB estimates the disturbance in the acceleration dimension ($\ddot{\boldsymbol{x}}^{\boldsymbol{dis}} = \left[{}^{w}\ddot{x}^{dis}\ {}^{w}\ddot{y}^{dis}\ 0\right]^T$) to the vehicle from the acceleration reference ($\ddot{\boldsymbol{x}}^{\boldsymbol{ref}}$) and the velocity response ($\dot{\boldsymbol{x}}^{\boldsymbol{res}}$) in world coordinates. Among the estimated disturbances, disturbance compensation in the turning direction was not performed, given the interference with the VTVC. By using the transformation matrix ${}^{\boldsymbol{w}}\boldsymbol{R_v}$ and

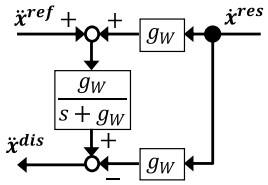

FIGURE 6. Block diagram of the WOB.

selection matrix $\boldsymbol{S}$, the disturbance estimated by the WOB is decomposed into translational disturbance ${}^{\boldsymbol{v}}\ddot{\boldsymbol{x}}^{\boldsymbol{dis}}_{\boldsymbol{tr}}$ and lateral disturbance ${}^{\boldsymbol{v}}\ddot{\boldsymbol{x}}^{\boldsymbol{dis}}_{\boldsymbol{la}}$, as follows:

$${}^{\boldsymbol{v}}\ddot{\boldsymbol{x}}^{\boldsymbol{dis}}_{\boldsymbol{tr}} = (\boldsymbol{I} - \boldsymbol{S})\,{}^{\boldsymbol{w}}\boldsymbol{R_v}\ddot{\boldsymbol{x}}^{\boldsymbol{dis}} = \left[{}^{v}\ddot{x}^{dis}\ 0\ 0\right]^T, \tag{25}$$

$${}^{\boldsymbol{v}}\ddot{\boldsymbol{x}}^{\boldsymbol{dis}}_{\boldsymbol{la}} = \boldsymbol{S}\,{}^{\boldsymbol{w}}\boldsymbol{R_v}\ddot{\boldsymbol{x}}^{\boldsymbol{dis}} = \left[0\ {}^{v}\ddot{y}^{dis}\ 0\right]^T, \tag{26}$$

$$\boldsymbol{S} = diag\left[0\ 1\ 0\right]. \tag{27}$$

The translational disturbance ${}^{\boldsymbol{v}}\ddot{\boldsymbol{x}}^{\boldsymbol{dis}}_{\boldsymbol{tr}}$ can be suppressed by feeding them back to the acceleration reference in the world coordinates. The lateral disturbance ${}^{\boldsymbol{v}}\ddot{\boldsymbol{x}}^{\boldsymbol{dis}}_{\boldsymbol{la}}$ is equivalent to the effects of lateral slippage and nonholonomic constraints. In this study, the lateral disturbance was defined as the equivalent lateral disturbance. The direct feedback of the equivalent lateral disturbance ${}^{\boldsymbol{v}}\ddot{\boldsymbol{x}}^{\boldsymbol{dis}}_{\boldsymbol{la}}$ does not suppress it because of nonholonomic constraints. Therefore, we propose VTVC to suppress equivalent lateral disturbances.

In the VTVC, the equivalent lateral disturbance is indirectly suppressed by ensuring that the turning velocity follows the virtual-turning velocity reference, defined using the equivalent lateral disturbance and vehicle velocity. The vehicle should turn to generate a velocity opposite the direction of the disturbance to indirectly compensate for the equivalent lateral disturbance. For a sufficiently small slip angle ϕ', the following equation can be derived by transforming the equation of motion expressed by (6) using the turning velocity and slipping angular velocity:

$$mv_x(\dot{\phi} - \dot{\phi}') = F_y = m{}^{v}\ddot{y}^{dis}. \tag{28}$$

Therefore, the velocity reference to compensate for the equivalent lateral disturbance is defined as the virtual-turning velocity reference $\dot{\phi}_{vt}^{ref}$ as follows:

$$\dot{\phi}_{vt}^{ref} = \frac{{}^{v}\ddot{y}^{dis}}{v_x}. \tag{29}$$

In practice, oscillatory variation should be considered because of the division between velocity and acceleration. Therefore, the experimentally determined virtual-turning velocity gain K_{vt} and threshold $\dot{\phi}_{vt}^{lim}$ are expressed by

$$\dot{\phi}_{vt}^{ref} = K_{vt}\frac{{}^{v}\ddot{y}^{dis}}{v_x}, \tag{30}$$

$$|\dot{\phi}_{vt}^{ref}| \leq \dot{\phi}_{vt}^{lim}. \tag{31}$$

The velocity controller is then designed as follows:

$$\ddot{\boldsymbol{x}}^{\boldsymbol{ref_v}} = [* \ * \ \ddot{\phi}^{ref}]^T = \boldsymbol{C_v}(\boldsymbol{s})(\dot{\phi}_{vt}^{ref} - \dot{\phi}^{res}), \tag{32}$$

where $\ddot{\boldsymbol{x}}^{\boldsymbol{ref_v}}$ and $\ddot{\phi}^{ref}$ are the acceleration reference vector generated by the velocity controller and its turning direction component, respectively. The velocity controller $\boldsymbol{C_v}(\boldsymbol{s})$ was designed using proportional control, as follows:

$$\boldsymbol{C_v}(\boldsymbol{s}) = K_{vp}, \tag{33}$$

where K_{vp} is a scalar parameter representing the proportional gain in the velocity. The equivalent lateral disturbance is indirectly compensated for by ensuring that the turning velocity of the tracked vehicle follows the virtual-turning velocity reference.

D. DRIVING FORCE CONTROL

The acceleration reference vector in the world coordinates is obtained using the outputs of the position and velocity controllers and the translational direction disturbance, as follows:

$$\ddot{\boldsymbol{x}}^{\boldsymbol{ref}} = \ddot{\boldsymbol{x}}^{\boldsymbol{ref_p}} + \ddot{\boldsymbol{x}}^{\boldsymbol{ref_v}} + {}^{v}\boldsymbol{R_w}\,{}^{v}\ddot{\boldsymbol{x}}_{\boldsymbol{tr}}^{\boldsymbol{dis}}. \tag{34}$$

The acceleration reference in (34) is transformed into the vehicle coordinates $\dot{\boldsymbol{v}}^{\boldsymbol{ref}}$ using the command conversion matrix $\boldsymbol{T}$. From this acceleration reference, the driving force reference $\boldsymbol{F}_{\boldsymbol{dr}}^{\boldsymbol{ref}}$ for each crawler is obtained using the distribution method described in Section III. The force controller was designed to feed back the driving force estimated by the DFOB and track the force reference, as follows:

$$\boldsymbol{F}_{\boldsymbol{mt}}^{\boldsymbol{ref}} = \boldsymbol{C_f}(\boldsymbol{s})(\boldsymbol{F}_{\boldsymbol{dr}}^{\boldsymbol{ref}} - \hat{\boldsymbol{F}}_{\boldsymbol{dr}}), \tag{35}$$

The force controller $\boldsymbol{C_f}(\boldsymbol{s})$ was designed using proportional-integral control, as follows:

$$\boldsymbol{C_f}(\boldsymbol{s}) = \boldsymbol{K_{fp}} + \frac{1}{s}\boldsymbol{K_{fi}}, \tag{36}$$

where $\boldsymbol{K_{fp}}$ and $\boldsymbol{K_{fi}}$ are the proportional and integral gains in the driving force, respectively.

V. EXPERIMENTS

A. EXPERIMENTAL CONDITIONS

We present the results of three experiments conducted to verify the effect of the driving force distribution on turning, the effect of the VTVC on the equivalent lateral disturbance suppression and position control, and the positioning performance for different trajectories. Fig. 7 shows the experimental setup, and Table 2 lists the specifications for the experimental setup. The experimentally tracked vehicle was driven by two direct-current motors with encoders. The tracked vehicle was equipped with an inertial measurement unit (IMU) to measure the acceleration and angular velocity. The Kalman filter was applied to the measured acceleration and angular velocity to estimate the turning angle. An augmented reality (AR) marker was installed on the surface of the vehicle. The vehicle position was measured by detecting the AR marker from the images captured using a camera. Based on previous trials, the number of neurons in the hidden layer of the TVNN was determined to be 15. The TVNN was trained using the Bayesian regularization error backpropagation method based on the velocity measured by detecting the AR marker as the supervisory data.

B. TURNING EVALUATION VIA DRIVING FORCE DISTRIBUTION

First, we evaluated the turning performance based on the driving force distribution. The proposed driving force distribution was compared with the method used in [30], described by a distribution matrix $\boldsymbol{D}$ consisting of a square Jacobian $\boldsymbol{J}$ and an equivalent inertia matrix $\boldsymbol{M_n}$, as follows:

$$\boldsymbol{D} = \frac{\boldsymbol{J}^{-1}\boldsymbol{M_n}}{R}, \tag{37}$$

$$\boldsymbol{M_n} = R^2\begin{bmatrix} \frac{m}{4} + \frac{J}{W^2} + \frac{J_m}{R^2} & \frac{m}{4} - \frac{J}{W^2} \\ \frac{m}{4} - \frac{J}{W^2} & \frac{m}{4} + \frac{J}{W^2} + \frac{J_m}{R^2} \end{bmatrix} \tag{38}$$

The position command vector ($\boldsymbol{x}^{\boldsymbol{cmd}} = \begin{bmatrix} x^{cmd} & y^{cmd} & \phi^{cmd} \end{bmatrix}^T$) is expressed as a function of time t, where

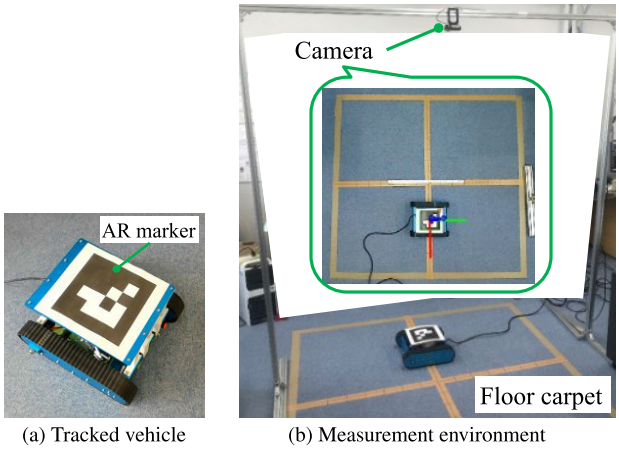

(a) Tracked vehicle (b) Measurement environment

FIGURE 7. Experimental setup.

$\boldsymbol{x}^{cmd} = [0\ m\ 0\ m\ \pi t/10\ rad]^T$. The control parameters are listed in Table 3. For comparison, the position response, including the turning angle response, was fed back directly instead of the VTVC.

Figs. 8 and 9 show the tracking performance in the turning direction using the distribution matrix $\boldsymbol{D}$ and the proposed driving force distribution, respectively. In Figs. 8 and 9, panels (a) and (b) represent the turning angle and driving force of the crawler, respectively. In Fig. 8 (a), poor turning performance is shown using the distribution matrix. As shown in Fig. 8 (b), the driving forces of the crawlers ($\hat{F}_{dr,r}$, $\hat{F}_{dr,l}$) follow the references ($F^{ref}_{dr,r}$, $F^{ref}_{dr,l}$). However, this result suggests that the driving forces of the crawlers changed simultaneously, indicating that the driving forces interfere with each other. Consequently, the driving force interference hinders the generation of the moment necessary for turning. Conversely, the turning angle suitably follows the given command (Fig. 9 (a)). In Fig. 9 (b), the left and right driving forces are generated separately. This result indicates that the driving force is distributed to prevent interference. Therefore, turning can be improved by decoupling the driving forces of the crawlers using the proposed driving force distribution.

C. POSITION CONTROL EVALUATION BY VTVC

Next, we evaluated the position-tracking performance and disturbance suppression of the proposed system. Cases with and without this control were compared and evaluated to demonstrate the effectiveness of the introduced VTVC. The linear trajectory is expressed by $\boldsymbol{x}^{cmd} = [0.05 + 0.05t\ -\ 0.025 + 0.025t\ *]^T$. The initial position vector ($\boldsymbol{x}^{ini} = \left[x^{ini}\ y^{ini}\ \phi^{ini}\right]^T$) differs from the initial position command $\boldsymbol{x}^{ini} = [0\ m\ 0\ m\ 0\ rad]^T$. In this experiment, the turning angle command was neglected to control the virtual-turning velocity. The parameters used in this experiment are listed in Table 4. To determine the slippage of the tracked vehicle,

TABLE 2. Specifications of the experimental devices.

Parameters	Value
Mass of tracked vehicle m	5.3 kg
Thread of tracked vehicle W	0.24 m
Motor-shaft conversion moment of inertia J_m	3.1 E-06 kgm^2
Radius of sprocket R	0.05 m
Torque constant of the motor	0.0134 Nm/A
Motor encoder resolution	3072 PPR
Sampling time	3 ms
Camera frame rate	60 fps

TABLE 3. Control parameters for the turning control evaluation.

Parameters	Value
Position P gain $\boldsymbol{K_{pp}}$	diag[100 100 9]
Position D gain $\boldsymbol{K_{pd}}$	diag[20 20 6]
Force P gain $\boldsymbol{K_{fp}}$	diag[0.2 0.2]
Force I gain $\boldsymbol{K_{fi}}$	diag[500 500]
Cutoff frequency of DOB	188.4 rad/s
Cutoff frequency of DFOB g_{DF}	188.4 rad/s
Cutoff frequency of WOB g_W	31.4 rad/s

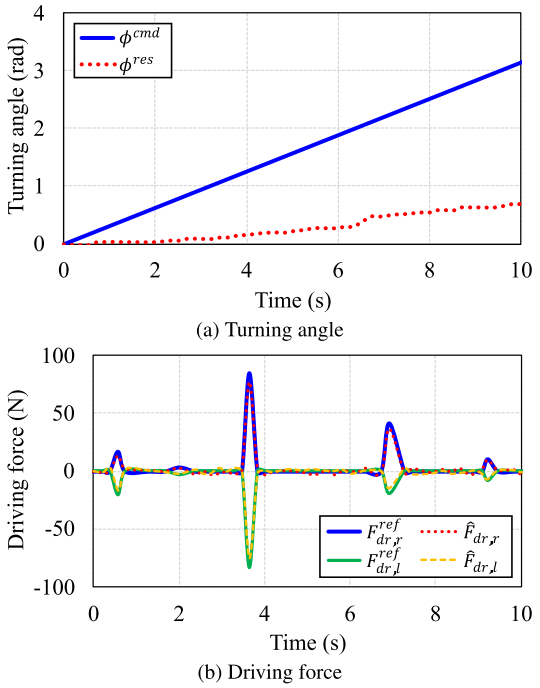

FIGURE 8. Turning performance using the proposed driving force distribution.

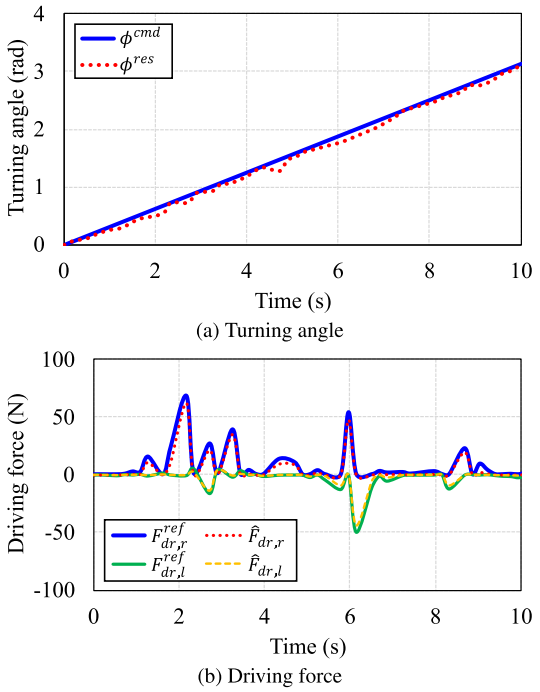

FIGURE 9. Turning performance using the proposed driving force distribution.

we compared the response coordinates (x^{res}, y^{res}) calculated from the crawler motor encoders and IMU with the absolute coordinates (x^{meas}, y^{meas}) obtained from the detected AR marker position.

Figs. 10 and 11 show the performances without and with VTVC, respectively. Panels (a), (b), and (c) show

TABLE 4. Control parameters for the position control evaluation.

Parameters	Value
Position P gain $\boldsymbol{K_{pp}}$	diag[100 100 0]
Position D gain $\boldsymbol{K_{pd}}$	diag[20 20 0]
Force P gain $\boldsymbol{K_{fp}}$	diag[0.2 0.2]
Force I gain $\boldsymbol{K_{fi}}$	diag[500 500]
Cutoff frequency of DOB	188.4 rad/s
Cutoff frequency of DFOB g_{DF}	188.4 rad/s
Cutoff frequency of WOB g_W	31.4 rad/s
Virtual-turning velocity gain K_{vt}	0.1
Velocity P gain K_{vp}	1.0
Limit virtual-turning velocity $\dot{\phi}_v^{lim}$	10 rad/s

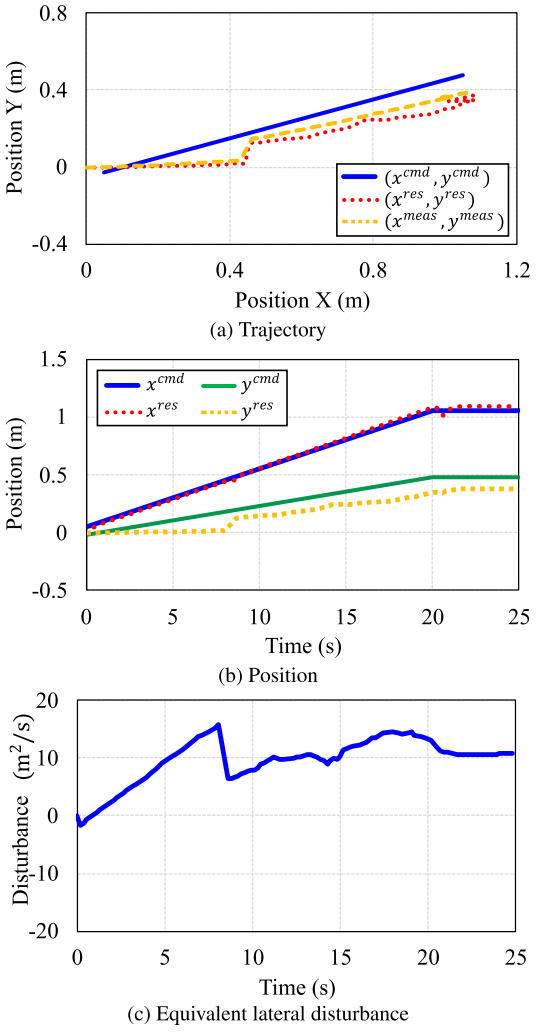

FIGURE 10. Tracking performance without the VTVC.

the trajectory tracking, position response, and equivalent lateral disturbance, respectively. A comparison of Figs. 10 (a) and 11 (a) shows that the VTVC improved the trajectory tracking and reduced the error between the absolute and estimated coordinates. From Figs. 10 (b) and 11 (b), the tracking performance along the Y_w-axis was improved using the VTVC. Furthermore, a comparison of Figs. 10 (c) and 11 (c) shows the effect of the VTVC on the equivalent lateral disturbance suppression. Without the

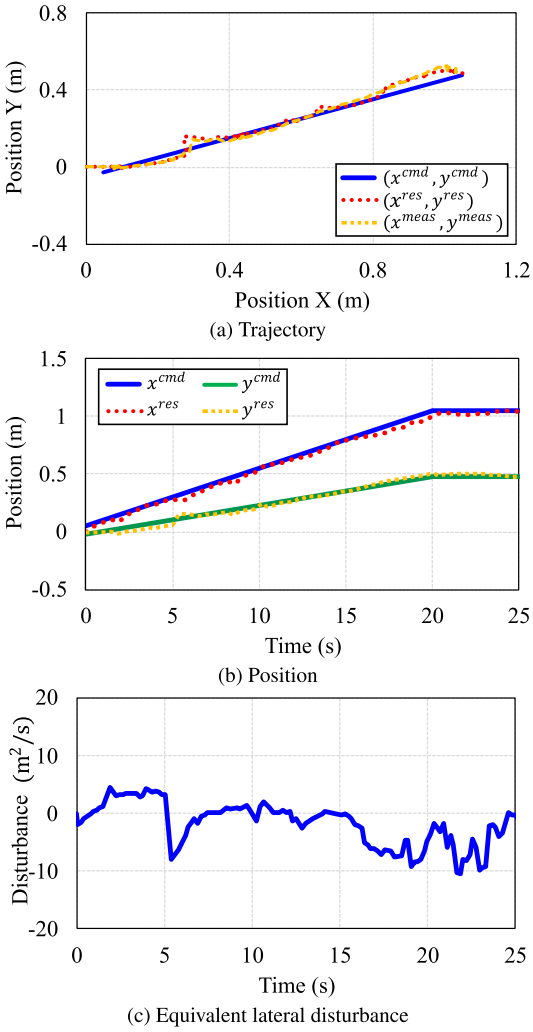

FIGURE 11. Tracking performance with the VTVC.

VTVC, the effect of the equivalent lateral disturbance was evident, particularly in terms of lateral positioning. Conversely, the positioning performance was likely improved by suppressing the equivalent lateral disturbance using the VTVC. Furthermore, the performance of self-positioning estimation could be improved by appropriately suppressing slippage because the difference between the absolute and response coordinates decreased with the introduction of the VTVC. These results confirm that the proposed control system improves the positioning performance of the tracked vehicle while appropriately allowing for slippage in the turning direction.

D. TRACKING AND SELF-POSITIONING PERFORMANCES EVALUATION FOR DIFFERENT TRAJECTORIES

Finally, we evaluated the tracking and self-positioning performances for various trajectories. The position commands listed in Table 5 are expressed as trajectories for 20 s. The same control parameters were used in this evaluation, as listed in Table 4. The initial position vector $\boldsymbol{x}^{ini}$ was set the same as the initial value of the position command

TABLE 5. Position commands.

Trajectory	x^{cmd}
Quadratic curve	$[0.04t\ 0.008t^2\ *]^T$
Circle	$[0.4\sin(0.1\pi t)\ -0.4\cos(0.1\pi t)\ *]^T$

TABLE 6. Positioning performances.

	Maximum error	Average error	Standard deviation
Quadratic curve	0.054 m	0.023 m	0.014 m
Circle	0.072 m	0.028 m	0.016 m

TABLE 7. Self-position estimation performances.

	Maximum error	Average error	Standard deviation
Quadratic curve	0.031 m	0.017 m	0.007 m
Circle	0.032 m	0.017 m	0.008 m

vector. Here, the norms between the absolute coordinates (x^{meas}, y^{meas}) and the position command (x^{cmd}, y^{cmd}) at each sampling were treated as positioning errors. The norms between the position response (x^{res}, y^{res}) and the absolute coordinates (x^{meas}, y^{meas}) at each sampling were treated as self-positioning estimation errors.

Tables 6 and 7 list the data for the positioning errors and self-positioning estimation errors for each trajectory, respectively. Table 6 confirms that the positioning performance of the proposed system is comparable for different trajectories. Furthermore, Table 7 indicates that the self-position estimation errors decrease, independent of the trajectory. The slight difference between the absolute and response coordinates suggests that the slippage was suppressed sufficiently.

VI. CONCLUSION

We proposed a driving force distribution to control a tracked vehicle and VTVC to suppress the equivalent lateral disturbance. First, the crawler driving force control suppressed slippage in the translational direction of the tracked vehicle. Next, the proposed driving force distribution enabled the decoupling of the crawlers using the instantaneous turning center of the vehicle to induce adequate slippage in the turning direction. Furthermore, the VTVC suppressed the equivalent lateral disturbance. The experimental results confirmed that the position tracking performance was improved by suppressing the lateral disturbance while allowing the tracked vehicle to slip adequately.

The proposed position control method can be applied to mobile robots in general, where the occurrence of slippage cannot be disregarded. The position control proposed in this paper does not consider the case where there are obstacles in the path. In the future, we aim to study countermeasures such as a position control method that includes obstacle avoidance.

REFERENCES

[1] A. Honda, H. Kato, and T. Tsumaki, "Development of simulation system for multi-pair crawlered and transforming explorer," in *Proc. IEEE Aerosp. Conf.*, Big Sky, MT, USA, Mar. 2015, pp. 1–8, doi: 10.1109/AERO.2015.7119030.

[2] K. Kawabata and K. Suzuki, "Development of a robot simulator for remote operations for nuclear decommissioning," in *Proc. 16th Int. Conf. Ubiquitous Robots (UR)*, Jeju, South Korea, Jun. 2019, pp. 501–504, doi: 10.1109/URAI.2019.8768640.

[3] H. Kuwahara, K. Hiraguri, and F. Terai, "Development of pushing control mechanisms for generator inspection robot," in *Proc. IEEE 16th Int. Workshop Adv. Motion Control (AMC)*, Kristiansand, Norway, Sep. 2020, pp. 135–142, doi: 10.1109/AMC44022.2020.9244480.

[4] K. H. Cho, Y. H. Jin, H. M. Kim, H. Moon, J. C. Koo, and H. R. Choi, "Multifunctional robotic crawler for inspection of suspension bridge hanger cables: Mechanism design and performance validation," *IEEE/ASME Trans. Mechatronics*, vol. 22, no. 1, pp. 236–246, Feb. 2017, doi: 10.1109/TMECH.2016.2614578.

[5] Y. Xia, M. Fu, C. Li, F. Pu, and Y. Xu, "Active disturbance rejection control for active suspension system of tracked vehicles with gun," *IEEE Trans. Ind. Electron.*, vol. 65, no. 5, pp. 4051–4060, May 2018, doi: 10.1109/TIE.2017.2772182.

[6] S. Morita, T. Hiramatsu, M. Niccolini, A. Argiolas, and M. Ragaglia, "Kinematic track modelling for fast multiple body dynamics simulation of tracked vehicle robot," in *Proc. 23rd Int. Conf. Methods Models Autom. Robot. (MMAR)*, Miedzyzdroje, Poland, Aug. 2018, pp. 910–915, doi: 10.1109/MMAR.2018.8486133.

[7] Z. Jinzheng, J. Qichun, W. Qi, and Z. Peng, "Analysis and simulation of interaction mechanism between agricultural tracked vehicle and ground," in *Proc. Int. Conf. Comput. Syst., Electron. Control (ICCSEC)*, Dalian, China, Dec. 2017, pp. 178–182, doi: 10.1109/ICCSEC.2017.8446867.

[8] Z. Qin, L. Chen, J. Fan, B. Xu, M. Hu, and X. Chen, "An improved real-time slip model identification method for autonomous tracked vehicles using forward trajectory prediction compensation," *IEEE Trans. Instrum. Meas.*, vol. 70, pp. 1–12, Jan. 2021, doi: 10.1109/TIM.2020.3048801.

[9] X. Ding, Z. Wang, L. Zhang, and C. Wang, "Longitudinal vehicle speed estimation for four-wheel-independently-actuated electric vehicles based on multi-sensor fusion," *IEEE Trans. Veh. Technol.*, vol. 69, no. 11, pp. 12797–12806, Nov. 2020, doi: 10.1109/TVT.2020.3026106.

[10] Y. Wang, B. M. Nguyen, H. Fujimoto, and Y. Hori, "Multirate estimation and control of body slip angle for electric vehicles based on onboard vision system," *IEEE Trans. Ind. Electron.*, vol. 61, no. 2, pp. 1133–1143, Feb. 2014, doi: 10.1109/TIE.2013.2271596.

[11] M. Salah and A. Al-Jarrah, "Robust backstepping control for tracked vehicles under the influence of slipping and skidding," in *Proc. 20th Int. Conf. Res. Educ. Mechatronics (REM)*, Wels, Austria, May 2019, pp. 1–6, doi: 10.1109/REM.2019.8744096.

[12] M. Chae, Y. Hyun, K. Yi, and K. Nam, "Dynamic handling characteristics control of an in-Wheel-Motor driven electric vehicle based on multiple sliding mode control approach," *IEEE Access*, vol. 7, pp. 132448–132458, 2019, doi: 10.1109/ACCESS.2019.2940434.

[13] Z. Ziye, L. Haiou, C. Huiyan, X. Shaohang, and L. Wenli, "Tracking control of unmanned tracked vehicle in off-road conditions with large curvature," in *Proc. IEEE Intell. Transp. Syst. Conf. (ITSC)*, Auckland, New Zealand, Oct. 2019, pp. 3867–3873, doi: 10.1109/ITSC.2019.8917468.

[14] M. Chen, "Disturbance attenuation tracking control for wheeled mobile robots with skidding and slipping," *IEEE Trans. Ind. Electron.*, vol. 64, no. 4, pp. 3359–3368, Apr. 2017, doi: 10.1109/TIE.2016.2613839.

[15] J. Kim and B. K. Kim, "Cornering trajectory planning avoiding slip for differential-wheeled mobile robots," *IEEE Trans. Ind. Electron.*, vol. 67, no. 8, pp. 6698–6708, Aug. 2020.

[16] J. Y. Wong, *Theory of Ground Vehicles*, 4th ed. New York, NY, USA: Wiley, 2008, pp. 147–156.

[17] K. Nagatani, D. Endo, and K. Yoshida, "Improvement of the odometry accuracy of a crawler vehicle with consideration of slippage," in *Proc. IEEE Int. Conf. Robot. Automat.*, Rome, Italy, Apr. 2007, pp. 2752–2757, doi: 10.1109/ROBOT.2007.363881.

[18] L. Zhai, X. Zhang, Z. Wang, Y. M. Mok, R. Hou, and Y. Hou, "Steering stability control for four-motor distributed drive high-speed tracked vehicles," *IEEE Access*, vol. 8, pp. 94968–94983, 2020, doi: 10.1109/ACCESS.2020.2995520.

[19] J. Huang, Y. Liu, M. Liu, M. Cao, and Q. Yan, "Multi-objective optimization control of distributed electric drive vehicles based on optimal torque distribution," *IEEE Access*, vol. 7, pp. 16377–16394, 2019, doi: 10.1109/ACCESS.2019.2894259.

[20] T. Hsiao, "Robust wheel torque control for traction/braking force tracking under combined longitudinal and lateral motion," *IEEE Trans. Intell. Transp. Syst.*, vol. 16, no. 3, pp. 1335–1347, Jun. 2015, doi: 10.1109/TITS.2014.2361515.
[21] Y. Wang, H. Fujimoto, and S. Hara, "Driving force distribution and control for EV with four in-wheel motors: A case study of acceleration on split-friction surfaces," *IEEE Trans. Ind. Electron.*, vol. 64, no. 4, pp. 3380–3388, Apr. 2017, doi: 10.1109/TIE.2016.2613838.
[22] Z. Sun, Y. Xia, L. Dai, K. Liu, and D. Ma, "Disturbance rejection MPC for tracking of wheeled mobile robot," *IEEE/ASME Trans. Mechatronics*, vol. 22, no. 6, pp. 2576–2587, Dec. 2017, doi: 10.1109/TMECH.2017.2758603.
[23] H. Kuwahara and T. Murakami, "Tracked vehicle velocity estimation by disturbance observer and machine learning, and its application to driving force control for slippage suppression," *IEEJ J. Ind. Appl.*, vol. 11, no. 1, pp. 69–75, Jan. 2022, doi: 10.1541/ieejjia.21002955.
[24] H. Kuwahara and T. Murakami, "Trajectory tracking control with estimated driving force for tracked vehicle using disturbance observer and machine learning," in *Proc. IEEE 30th Int. Symp. Ind. Electron. (ISIE)*, Kyoto, Japan, Jun. 2021, pp. 1–6, doi: 10.1109/ISIE45552.2021.9576259.
[25] K. Matsushita and T. Murakami, "Nonholonomic equivalent disturbance based backward motion control of tractor-trailer with virtual steering," *IEEE Trans. Ind. Electron.*, vol. 55, no. 1, pp. 280–287, Jan. 2008, doi: 10.1109/TIE.2007.908522.
[26] T. Shibata and T. Murakami, "Power-assist control of pushing task by repulsive compliance control in electric wheelchair," *IEEE Trans. Ind. Electron.*, vol. 59, no. 1, pp. 511–520, Jan. 2012, doi: 10.1109/TIE.2011.2146210.
[27] K. Ohishi, M. Nakao, K. Ohnishi, and K. Miyachi, "Microprocessor-controlled DC motor for load-insensitive position servo system," *IEEE Trans. Ind. Electron.*, vol. IE-34, no. 1, pp. 44–49, Feb. 1987, doi: 10.1109/TIE.1987.350923.
[28] E. Sariyildiz, R. Oboe, and K. Ohnishi, "Disturbance observer-based robust control and its applications: 35th anniversary overview," *IEEE Trans. Ind. Electron.*, vol. 67, no. 3, pp. 2042–2053, Mar. 2020, doi: 10.1109/TIE.2019.2903752.
[29] M. Kurisu, "Tracking control for a tracked vehicle based on prediction model of virtual wheeled robot," in *Proc. IEICE Int. Symp. Nonlinear Theory Appl. (NOLTA)*, Budapest, Hungary, Sep. 2008, pp. 21–24, doi: 10.34385/proc.42.A1L-C3.
[30] D. Saito and T. Murakami, "A turning control of electric wheeled Walker device by PSD camera information," in *Proc. IEEE 13th Int. Workshop Adv. Motion Control (AMC)*, Yokohama, Japan, Mar. 2014, pp. 616–620, doi: 10.1109/AMC.2014.6823352.

HIROAKI KUWAHARA (Member, IEEE) received the B.E. degree in system design engineering and the M.E. degree in integrated design engineering from Keio University, Yokohama, Japan, in 2008 and 2010, respectively, where he is currently pursuing the Ph.D. degree in integrated design engineering. Since 2010, he has been with the Corporate Manufacturing Engineering Center, Toshiba Corporation, Yokohama, where he is also a Researcher. From 2014 to 2015, he was also a Visiting Researcher with the Dynamic Legged Systems Laboratory, Istituto Italiano di Tecnologia (IIT), Genoa, Italy. His research interests include robotics, automation, and motion control.

TOSHIYUKI MURAKAMI (Senior Member, IEEE) received the B.E., M.E., and Ph.D. degrees in electrical engineering from Keio University, Yokohama, Japan, in 1988, 1990, and 1993, respectively. In 1993, he joined the Department of Electrical Engineering, Keio University. From 1999 to 2000, he was a Visiting Researcher with the Institute for Power Electronics and Electrical Drives, Aachen University of Technology, Aachen, Germany. He is currently a Professor with the Department of System Design Engineering, Keio University. In the education project, he was a Co-ordinator of the European Master on Advanced Robotics (EMARO), Erasmus Program, from 2008 to 2018. Since 2019, he has been a responsible person of the Japan Europe Master on Advanced Robotics (JEMARO), Erasmus, and MEXT Program with the Faculty of Science and Technology, Keio University. His research interests include robotics, intelligent vehicles, mobile robots, and motion control.